Osteoporosis: A multiscale modeling viewpoint

Conference Paper · September 2011

DOI: 10.1145/2037509.2037536 · Source: DBLP

4 authors:

Nicola Paoletti
Stony Brook University
48 PUBLICATIONS **169** CITATIONS
SEE PROFILE

Pietro Lio
University of Cambridge
379 PUBLICATIONS **6,835** CITATIONS
SEE PROFILE

Emanuela Merelli
University of Camerino
153 PUBLICATIONS **1,205** CITATIONS
SEE PROFILE

Marco Viceconti
The University of Sheffield
447 PUBLICATIONS **8,848** CITATIONS
SEE PROFILE

Osteoporosis: a multiscale modeling viewpoint

Nicola Paoletti
School of Science and Technology, Computer Science
University of Camerino
Camerino, IT
nicola.paoletti@unicam.it

Pietro Liò
Computer Laboratory
University of Cambridge
Cambridge, UK
pl219@cam.ac.uk

Emanuela Merelli
School of Science and Technology, Computer Science
University of Camerino
Camerino, IT
emanuela.merelli@unicam.it

Marco Viceconti
Laboratorio di Tecnologia Medica
Istituto Ortopedico Rizzoli
Bologna, IT
viceconti@tecno.ior.it

ABSTRACT

Our work focuses on bone remodeling with a multiscale breadth that ranges from modeling intracellular and intercellular RANK/RANKL signaling to tissue dynamics. Several important findings provide clear evidences of the multiscale properties of bone formation and of the links between RANK/RANKL and bone density in health and disease conditions. Recent studies indicate that the circulating levels of OPG and RANKL are inversely related to bone turnover and bone mineral density (BMD) and contribute to the development of osteoporosis in postmenopausal women, and thalassemia-induced osteoporosis. We make use of a spatial process algebra, the Shape Calculus, to control stochastic cell agents that are continuously remodeling the bone. We found that our description is effective for such a multiscale, multilevel process and that RANKL signaling small dynamic concentration defects are greatly amplified by the continuous alternation of absorption and formation resulting in large structural bone defects.

Categories and Subject Descriptors

I.6 [**Simulation and Modeling**]: Model Validation and Analysis, Model Development; J.3 [**Life and Medical Sciences**]: Biology and genetics, Health

Keywords

osteoporosis, multiscale, shape calculus, bone remodeling, agent-based simulation

CMSB '11, September 21-23, 2011 Paris, FR

1. INTRODUCTION

Human cells have striking characteristics; their number of in the human body is thought to be close to 10^{14}, more than 1000 times the number of stars in the milky way. Instead the number of cell types is relatively small, about 200 but their diversity is remarkable large which explains the diversity of tissues and organs. One of the most important cell types are those in the skeleton affecting the *bone mineral density (BMD)*. The BMD used as a predictor of fracture, is a summation of the remodeling that occurs during growth and aging on the periosteal and endosteal (endocortical, intracortical, trabecular) surfaces of bone.

An important factor affecting bone metabolism is *RANK/RANKL/OPG signaling*. RANK is a protein expressed by *osteoclasts*, the cells responsible for bone resorption. RANK is a receptor for RANKL, a protein produced by *osteoblasts*, the cells responsible for bone formation. RANK/RANKL binding induces osteoclast differentiation, proliferation and activation, thus it prominently affects the resorption phase during bone remodeling. Osteoprotegerin (OPG) is a decoy receptor for RANKL. It is expressed by mature osteoblasts and it binds with RANKL, thus inhibiting the production of osteoclasts. Several important findings provide clear evidences of the multiscale properties of bone formation and of the links between RANK/RANKL and bone density in health and disease conditions. There is a lack of knowledge on the genetic and environmental factors responsible for age, gender specific differences in bone fragility and fracture rates. Recent studies indicate that the circulating levels of OPG and RANKL are inversely related to bone turnover and BMD and contribute to the development of osteoporosis in postmenopausal women [18], and thalassemia-induced osteoporosis [26].

This paper focuses on bone remodeling and has a multiscale breadth that ranges from modeling intracellular and intercellular RANK/RANKL signaling to tissue dynamics. With respect to our previous work [23], we simulate and compare healthy and pathological conditions, demonstrating that small changes in RANKL concentration lead to osteoporosis, especially when aging factors are involved.

We make use of a multilevel approach combining a high-level process-algebraic specification in the Shape Calculus, and a low-level stochastic agent-based simulation. The Shape Calculus provides the actual methodology to formally describe processes (cells) moving and interacting in the space (portion of bone tissue). On the other hand, the agent-based model represents the concretisation of the process-algebraic specification, and it is equipped with additional features such as *stochasticity* and *perception*. Although these features could have been added also at the specification level, we preferred to introduce them only at the implementation level. The reason is that we employ the Shape Calculus as a high-level specification language, which should be kept more generic as possible in order to be suitable for describing a large variety of biological and physical systems. Hence stochasticity and perception become significant and useful during the simulation of the model, not in its description.

Apart from the methodological novelties, the main contributions of this work are: a) a process-algebraic formulation and a runnable agent-based model for bone remodeling; b) the assessment of pathological conditions, by analyzing the results of the simulation.
The paper is organized as follows. Section 2 introduces the process of bone remodeling. In Section 3 we present the high-level specification of bone remodeling in the language of the Shape Calculus. In Section 4 we describe the stochastic agent-based simulator. In Section 5, we analyze the results of the simulation, considering healthy and osteoporotic scenarios. Finally, in Section 6 we compare our approach with other mathematical and computational methods used in bone remodeling, and we discuss future works.

2. MECHANICS OF BONE REMODELING

There are two main types of bone: 1) Compact tissue forms the outer shell of bones. It consists of a very hard (virtually solid) mass of bony tissue arranged in concentric layers (Haversian systems); 2) Cancellous (also known as "spongy") tissue is located beneath the compact bone and consists of a meshwork of bony bars (trabeculae) with many interconnecting spaces containing bone marrow. In the process of bone remodeling (BR), old bone is continuously replaced by new tissue [24]; this ensures that the mechanical integrity of the bone is maintained and, in healthy conditions, there are no global changes in the morphology. However, pathological conditions can alter the equilibrium between bone resorption and bone formation; osteoporosis is an example of negative remodeling: the resorption process prevails on the formation one and this reduces bone density, so increasing the risk of spontaneous fractures. Hence, the definition of faithful models for BR has a high social and clinical relevance in the prediction of bone diseases [14]. The bone remodeling process is conducted by *osteoclasts* and *osteoblasts*, forming Basic Multi-cellular Units (BMUs). Osteoblasts follow osteoclasts in a highly coordinated manner indicates that a coupled regulative mechanism must exist. It was suggested [20] that BMU activity is controlled by osteocytes in the bone matrix, serving as mechanosensors, sending signals through the osteocytic canalicular network to the BMU cells. Each BMU has a finite lifetime, so new units are continuously forming as old units are finishing [20].

In normal bone, the number of BMUs, the bone resorption rate, and the bone formation rate are all relatively constant [32]; while the key events during the BR could be summarised as below:

- the RANKL/RANK signaling regulates osteoclast formation, activation and survival in normal bone modeling and remodeling and in a variety of pathologic conditions characterized by increased bone turnover. OPG protects bone from excessive resorption by binding to RANKL and preventing it from binding to RANK. The relative concentration of RANKL in bone is a major determinant of bone mass and strength [16].
- the pre-osteoclasts circulate in the blood vessels if a new crack appears, the osteocytes near the crack undergo apoptosis osteocytes detect strain.
- the pre-osteoblasts start to express RANKL on their surfaces. Pre-osteoclasts have RANK receptors on their surfaces.
- the lining cells around the bone pull away from the bone matrix and form a canopy which merges with the blood vessels.
- the pre-osteoclasts enlarge and fuse into mature osteoclasts
- in cortical BMUs, osteoclasts excavate cylindrical tunnels in the predominant loading direction of the bone. They are followed by osteoblasts, filling the tunnel, creating secondary osteons of renewed tissue.
- the trabecular bone remodeling is mainly a surface event, in which osteoclasts dig a trench rather than a tunnel.

3. BONE REMODELING IN THE SHAPE CALCULUS

In this section we provide a brief introduction to the Shape Calculus, a bio-inspired spatial process calculus for describing 3D processes moving, colliding and interacting in a 3D space.
In few words, a 3D process is characterized by an *internal behavior* specified in a timed variant of *CCS (Calculus of Communicating Systems)* [25]; and by a so-called *3D shape*, defining the geometry and the physical properties of the process. In Table 3, the syntax of the calculus is presented.

The set $\mathbb{S}$ of **3D shapes** is composed of basic shapes σ, defined as a tuple $\sigma = \langle V, m, \mathbf{p}, \mathbf{v} \rangle$ (geometry, mass, position, velocity); and by compound shapes of the form $S_1 \langle X \rangle S_2$, resulting from the binding of two 3D shapes S_1 and S_2 on a common surface X. Shapes move according to their velocities that are determined by a general motion law - for instance as in a force field or Brownian motion - and by the collisions occurring among shapes.
The internal **behavior** of a 3D process supports a *bind* action, with which processes can bind together forming a compound new process; and *split* actions for breaking bonds. The binding between 3D processes is modeled in a similar way to CCS communication on complementary channels; in the Shape Calculus, channels act as binding sites and are of the form $\langle \alpha, X \rangle$, where α is a channel name,

$S ::=$		**3D shape** ($\mathbb{S}$-term)
	$\sigma = \langle V, m, \mathbf{p}, \mathbf{v} \rangle$	Basic shape
	$S\langle X \rangle S$	Composed shape
$B ::=$		**Behavior** ($\mathbb{B}$-term)
	nil	Null behavior
	$\langle \alpha, X \rangle.B$	Bind
	$\omega(\alpha, X).B$	Weak split
	$\rho(L).B$	Strong split
	$\epsilon(t).B$	Delay
	$B + B$	Choice
	K	Process name
$P ::=$		**3D process** (3DP-term)
	$S[B]$	$S \in \mathbb{S}, B \in \mathbb{B}$
	$P\langle a, X \rangle P$	Composed 3D process
$N ::=$		**3D network** ($\mathbb{N}$-term)
	nil	Empty network
	P	$P \in$ 3DP
	$N \| N$	Parallel 3D processes

Table 1: Shape Calculus syntax

and X is the active surface. The set of channels is denoted with $\mathcal{C}$. Binding can occur only when two channels $c_1 = \langle \alpha, X \rangle$ and $c_2 = \langle \beta, Y \rangle$ are *compatible* (written $c_1 \sim c_2$), namely if $\alpha = \overline{\beta}$ (complementary channels name), and $X \cap Y \neq \emptyset$ (they share a common surface of contact). In addition, the Shape Calculus supports two basic actions for splitting an established bond: the *weak-split* $\omega(\alpha, X)$ (not-urgent, can be postponed) and the *strong-split* $\rho(L), L \subseteq \mathcal{C}$ (urgent, must be performed as soon as it is enabled). We denote the sets of weak-split actions and strong-split actions with $\omega(\mathcal{C}) = \{\omega(\alpha, X) | \langle \alpha, X \rangle \in \mathcal{C}\}$, and $\rho(\mathcal{C}) = \{\rho(\alpha, X) | \langle \alpha, X \rangle \in \mathcal{C}\}$, respectively.
The set 3DP of **3D processes** is composed of basic processes of the form $S[B]$, which are characterized by a behavior $B \in \mathbb{B}$ encapsulated in a 3D shape $S \in \mathbb{S}$; and by composed processes $P_1\langle a, X \rangle P_2$, where $P_1, P_2 \in$ 3DP, a is the name of the two compatible channels, and X is the surface of contact.
Finally, we define a **network of 3D processes** (3D network, for short) as the parallel composition of zero or more 3D processes. Given a finite set of indexes $I = \{1, \ldots, n\}$, we can alternatively write $(\|P_i)_{i \in I}$ or $(\|P_i)_{i=1}^n$, with $P_i \in$ 3DP, to denote the network that consists of all P_i with $i \in I$: $P_1 \| \ldots \| P_n$.
Table 2 and Table 3 show the Structural Operational Semantics (SOS) [29] rules for the $\mathbb{B}$-terms of the Shape Calculus. We refer the interested reader to papers [2, 3] for the complete semantics and for a broader view of the calculus.

Figure 1 depicts a possible evolution of the 3D network $P_0 \| P_1$, where $P_0 \stackrel{\text{def}}{=} S_0[B_0]$ and $P_1 \stackrel{\text{def}}{=} S_1[B_1]$. In the initial configuration P_0 can perform an input bind action on $\langle a, X \rangle$ (the green area of P_0), and P_1 can perform an output bind action on $\langle \overline{a}, Y \rangle$ (the pink part of P_1); formally, $S_0[B_0] \xrightarrow{\langle a, X \rangle} S_0[B_0']$ and $S_1[B_1] \xrightarrow{\langle \overline{a}, Y \rangle} S_1[B_1']$. If a collision between P_0 and P_1 brings the surfaces X and Y into contact, i.e. $X \cap Y = Z \neq \emptyset$, the channels $\langle a, X \rangle$ and $\langle \overline{a}, Y \rangle$ become compatible. Consequently, the two processes bind together, and the resulting compound process is denoted with $S_0[B_0']\langle a, Z \rangle S_1[B_1']$ (Fig. 1 (b)). Finally, Figure 1 (c) illustrates the 3D network after the composed process has

$$\textsc{Nil}_t \frac{}{\mathsf{nil} \overset{t}{\rightsquigarrow} \mathsf{nil}} \qquad \textsc{Str}_t \frac{}{\rho(L).B \overset{t}{\rightsquigarrow} \rho(L).B}$$

$$\textsc{Pref}_t \frac{\mu \in \mathcal{C} \cup \omega(\mathcal{C})}{\mu.B \overset{t}{\rightsquigarrow} \mu.B} \qquad \textsc{Sum}_t \frac{B_1 \overset{t}{\rightsquigarrow} B_1' \quad B_2 \overset{t}{\rightsquigarrow} B_2'}{B_1 + B_2 \overset{t}{\rightsquigarrow} B_1' + B_2'}$$

$$\textsc{Del}_t \frac{t' \geq t}{\epsilon(t').B \overset{t}{\rightsquigarrow} \epsilon(t' - t).B} \qquad \textsc{Def}_t \frac{B \overset{t}{\rightsquigarrow} B'}{K \overset{t}{\rightsquigarrow} B'} \text{ if } K \stackrel{\text{def}}{=} B$$

Table 2: SOS rules for temporal behavior of a shape.

$$\textsc{Pref}_a \frac{\mu \in \mathcal{C} \cup \omega(\mathcal{C})}{\mu.B \xrightarrow{\mu} B} \qquad \textsc{Del}_a \frac{B \xrightarrow{\mu} B'}{\epsilon(0).B \xrightarrow{\mu} B'}$$

$$\textsc{Sum}_a \frac{B_1 \xrightarrow{\mu} B'}{B_1 + B_2 \xrightarrow{\mu} B'} \qquad \textsc{Def}_a \frac{B \xrightarrow{\mu} B'}{K \xrightarrow{\mu} B'} \text{ if } K \stackrel{\text{def}}{=} B$$

$$\textsc{Str}_1 \frac{L = \{\langle \alpha, X \rangle\}}{\rho(L).B \xrightarrow{\rho(\alpha, X)} B} \qquad \textsc{Str}_2 \frac{L = \{\langle \alpha, X \rangle\} \cup L' \quad L' \neq \emptyset}{\rho(L).B \xrightarrow{\rho(\alpha, X)} \rho(L').B}$$

Table 3: SOS rules for the functional behavior of a shape

split, supposing that $B_0' \xrightarrow{\rho(a, X)} B_0''$, and $B_1' \xrightarrow{\rho(\overline{a}, Y)} B_1''$ that is, they can perform a strong split action on the previously established bond.

3.1 Formal specification of bone remodeling

In this work we enriched the current theory of the Shape Calculus with some new features, which are both inspired by biological evidence and driven by more pragmatical needs.

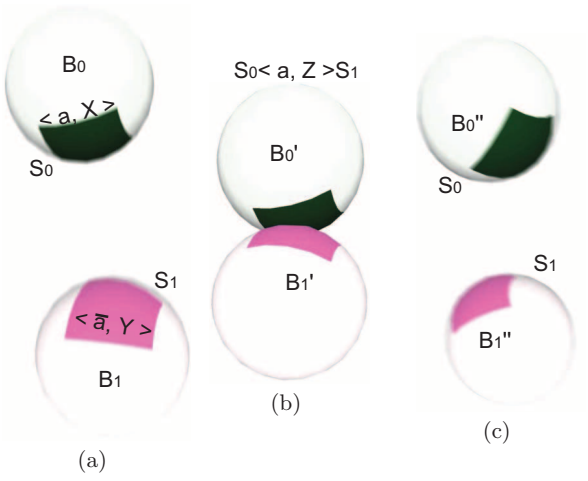

Figure 1: A possible evolution of the 3D network $S_0[B_0] \| S_1[B_1]$.

$$\textsc{Delta}_t \frac{B \overset{t'}{\rightsquigarrow} B' \quad t > t'}{\delta(t,B) \overset{t'}{\rightsquigarrow} \delta(t-t',B')} \qquad \textsc{Delta}_{t=0} \frac{t = t'}{\delta(t,B) \overset{t'}{\rightsquigarrow} \mathsf{nil}} \qquad \textsc{Delta}_a \frac{B \overset{\mu}{\rightarrow} B' \quad t > 0}{\delta(t,B) \overset{\mu}{\rightarrow} \delta(t,B')}$$

$$\textsc{Theta}_a \frac{}{\Theta.B \overset{\Theta}{\rightarrow} B} \qquad \textsc{Theta}_t \frac{}{\Theta.B \overset{t}{\rightsquigarrow} \Theta.B}$$

$$\textsc{Theta}_s \frac{S = \langle V, m, \mathbf{p}, \mathbf{v}\rangle \quad B \overset{\Theta}{\rightarrow} B' \quad S' = \langle\{\mathbf{p}\}, 0, \mathbf{p}, \mathbf{0}\rangle}{S[B] \overset{\Theta}{\rightarrow} S'[B']}$$

Table 4: SOS rules for the temporal and functional behavior of Θ and δ terms.

$(B)^k$ **Iteration:** a syntactical construct for expressing behaviors repeating for a finite or infinite number of iterations. Given $B \in \mathbb{B}$, $(B)^k$ is defined by the following:

$$(B)^k \equiv \begin{cases} B.(B)^k & \text{if } k = \infty \\ B.(B)^{k-1} & \text{if } k > 0,\ k \in \mathbb{N} \\ \mathsf{nil} & \text{if } k = 0,\ k \in \mathbb{N} \end{cases}$$

If B is an atomic term, we allow the notation B^k without parenthesis.

Θ **Thanatos:** in classical process algebras, a process terminates when it reaches a state where no further actions are possible; in the Shape Calculus, the behavior of a 3D process is enclosed in a formal shape which keeps existing, moving and (elastically) colliding even if its internal behavior reaches the termination state nil. From the necessity to describe phenomena like necrosis and apoptosis that are very common in cellular biology, especially in our model of the BMU, we defined a new behavioral term $\Theta \in \mathbb{B}$ (*thanatos*, a greek word for *death*), which is responsible for the "termination" of a 3D shape. Consider a process $P \overset{\text{def}}{=} S[B]$, where $S = \langle V, m, \mathbf{p}, \mathbf{v}\rangle$. Assuming that the transition $B \overset{\Theta}{\rightarrow} B'$ is fired, S is replaced by the shape $S' = \langle\{\mathbf{p}\}, 0, \mathbf{p}, (0,0,0)\rangle$, and all the bonds with other 3D processes are broken. In other words, S' is a sort of void shape, since it has null velocity and mass, and the set of its points V is only composed by the center $\mathbf{p}$. Consequently, the death of a 3D process is modeled with the sequence Θ.nil.

$\delta(t,B)$ **Behavior duration:** in order to properly express the fact that a behavior must be executed for a specific time interval (e.g. an osteoclast continuously mineralizes bone until its life time has passed), we introduced a new term $\delta(t,B) \in \mathbb{B}$, which models a time-bounded behavior. It is substantially different from the prefixing delay action $\epsilon(t).B$: while $t > 0$, $\delta(t,B) \equiv B$; once $t = 0$, $\delta(t,B) \equiv \mathsf{nil}$.

The operational semantics of Θ and $\delta(t,B)$ is illustrated in Table 4. In Table 6, the high-level Shape Calculus specification of the BMU model is presented. Notice that the model does not define particular binding surfaces for the channels exposed by the 3D processes, but we assume that their whole surface is available for binding. Let $\mathcal{B}(S)$ be the boundaries of a shape S; for the sake of succinctness, in our specification we will denote the channel $\langle \alpha, \mathcal{B}(S)\rangle$ with $\langle \alpha, X\rangle$. Furthermore, actions **resorb** and **form** are not encoded as behavioral terms, but they are implemented at the simulation level; they are responsible for decreasing/increasing the part of bone which the osteoclast/osteoblast is attached to.
Table 5 groups the numeric parameters of the Shape Calculus model, together with the references in which they occur.

Param	Value	Description
n_{Oc}	20 [21, 34]	Expected number of Oc
n_{Ob}	2000 [21, 34]	Expected number of Ob
t_{Oc}	10 days [34]	Oc lifetime
t_{Ob}	15 days [34]	Mature Ob lifetime
t_{Pb}	5 days [34]	Ob differentiation time

Table 5: Parameters of the Shape Calculus model

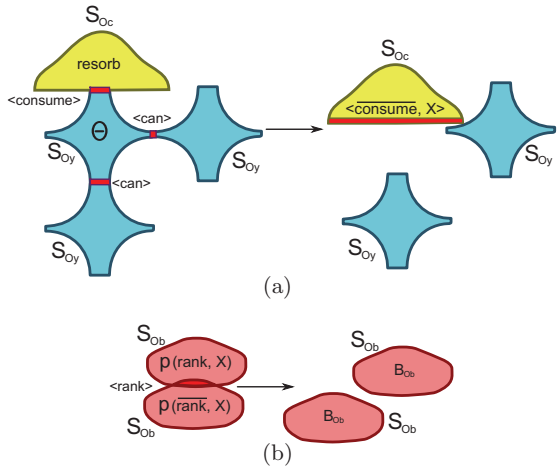

Figure 2: Graphical representation of some processes in the BMU 3D network. On the top, osteocytes are connected through the network of canaliculi; an osteoclast binds to an osteocyte, consuming it. The bottom figure shows the inhibition of a pre-osteoblast by a mature osteoblast, by binding/splitting on channel $\langle \mathsf{rank}, \cdot\rangle$.

4. STOCHASTIC AGENT-BASED IMPLEMENTATION

Traditionally, Systems Biology has been described by using ODEs, i.e. continuous deterministic mathematical models. A growing amount of experimental results is nowadays showing that biochemical kinetics at the single-cell level are intrinsically stochastic, suggesting that stochastic models are more effective in capturing the multiple sources of heterogeneity needed for modeling a biological dynamical system in a realistic way. In particular biological systems have also developed strategies for both exploiting and suppressing bi-

Tissue, BMU		
$Tissue$	$\stackrel{\text{def}}{=}$	$(\|ABMU_i)_{i=1}^{a} \parallel (\|QBMU_j)_{j=1}^{q}$
$ABMU$	$\stackrel{\text{def}}{=}$	$(\|Oy_i)_{i=1}^{n_{Oy}} \parallel (\|Oc_j)_{j=1}^{n_{Oc}} \parallel (\|Ob_k)_{k=1}^{n_{Ob}}$
$QBMU$	$\stackrel{\text{def}}{=}$	$(\|Oy_i)_{i=1}^{n_{Oy}}$

Bone tissue is structured in a active BMUs ($ABMU$) participating in the remodeling process, and in q quiescent BMUs ($QBMU$). Each active BMU is in turn composed by n_{Oy} osteocytes, n_{Oc} osteoclasts and n_{Ob} osteoblasts. An inactive BMU is modeled as a network of only osteocytes.

Osteocyte		
Oy	$\stackrel{\text{def}}{=}$	$S_{Oy}[(\langle \mathsf{can}, \mathsf{X}\rangle + \langle \overline{\mathsf{can}}, \mathsf{X}\rangle)^{\mathsf{k_{Oy}}} + \langle \mathsf{consume}, \mathsf{X}\rangle.\Theta]$

An osteocyte can bind with other $\mathsf{k_{Oy}}$ osteocytes through the channel $\langle \mathsf{can}, \cdot\rangle$ and form the network of canaliculi. Along a micro-fracture, they are not near enough to communicate with each other; hence, they expose channel $\langle \mathsf{consume}, \cdot\rangle$ which will activate the resorption phase. After having performed a bind on $\langle \mathsf{consume}, \cdot\rangle$, the osteocyte dies since it has been destroyed by the attached osteoclast (Fig. 2 (a)).

Osteoclast		
Oc	$\stackrel{\text{def}}{=}$	$S_{Oc}[\mathsf{B_{Oc}}]$
$\mathsf{B_{Oc}}$	$\stackrel{\text{def}}{=}$	$\delta(\mathsf{t_{Oc}}, (\langle \overline{\mathsf{consume}}, \mathsf{X}\rangle.\mathbf{resorb})^{\infty}).\Theta.\langle \mathsf{mineral}, \mathsf{X}\rangle^{\mathsf{k_{Oc}}}$

During its lifetime $\mathsf{t_{Oc}}$, an osteoclast continuously binds with osteocytes on channel $\langle \overline{\mathsf{consume}}, \cdot\rangle$ and resorb bone (Fig. 2 (a)). Before dying, it releases biochemical signals in order to attract osteoblasts to reconstruct that consumed part of bone. In particular, a single "dead" osteoclast can bind with $k_{Oc} = \lfloor \mathsf{n_{Ob}}/\mathsf{n_{Oc}} \rfloor$ osteoblasts, so fitting the ratio between active osteoclasts and active osteoblasts.

Osteoblast		
Ob	$\stackrel{\text{def}}{=}$	$S_{Ob}[\langle \overline{\mathsf{rank}}, \mathsf{X}\rangle.\rho(\overline{\mathsf{rank}}, \mathsf{X}).\mathsf{B_{OPG}} + \epsilon(\mathsf{t_{Pb}}).\mathsf{B_{OPG}}]$
$\mathsf{B_{OPG}}$	$\stackrel{\text{def}}{=}$	$\langle \mathsf{rank}, \mathsf{X}\rangle.\rho(\mathsf{rank}, \mathsf{X}).\mathsf{B_{Ob}} + \mathsf{B_{Ob}}$
$\mathsf{B_{Ob}}$	$\stackrel{\text{def}}{=}$	$\delta(\mathsf{t_{Ob}}, (\langle \overline{\mathsf{mineral}}, \mathsf{X}\rangle.\mathbf{form})^{\infty}).\Theta$

An osteoblast initially behaves as a non differentiated cell: it produces RANKL, by exposing channel $\langle \mathsf{rank}, \cdot\rangle$. After the effect of OPG-inihibition or after its differentiation time $\mathsf{t_{Pb}}$ has elapsed, it starts behaving as a mature osteoblast which produces OPG. In particular, an osteoblast can inihibit a single precursor, by binding on the channel $\langle \overline{\mathsf{rank}}, \cdot\rangle$ (Fig. 2 (b)). Then, the formation phase lasts a time $\mathsf{t_{Ob}}$, after which the cell undergoes apoptosis.

Table 6: Biological description and Shape Calculus specification

ological noise and heterogeneity. At present, there is a limited number of continuous models on bone remodeling [21, 34, 28] and a complete lack of stochastic models. The statistical fluctuations in RANKL concentrations in the blood microcirculation will produce changes in the chemotaxis, i.e. the process by which cells move toward attractant molecules, of osteoclasts and osteoblasts (for example, the cell differentiation, number and arrival time). Other important sources of variability are related to the time and space organisation of the BMU to the availability of molecules required for building the bone and to the regulatory feedback control and to the mechanical boundary conditions [13].

In this part, we introduce the agent-based simulator developed for running a single BMU, and we discuss some interesting features of our model. The most important peculiarities introduced are *stochastic actions* and the *distance sensibility*, the capability of an agent to perceive its neighborhood.

Stochasticity.

Following the approach in [12, 17], actions performed by the agents are equipped with *stochastic rates* and *weights*. In particular, *output actions* are annotated with a rate $\lambda \in \mathbb{R}^+$, characterizing a random variable with a negative exponential distribution, modeling the duration of the action. *Input actions* have associated a weight $\omega \in \mathbb{N}^+$ (not to be confused with the weak-split action of the Shape Calculus), representing the probability that the specific input is selected when a compatible output action is fired.

This stochastic framework characterized by a two-party synchronization and by passive input actions has been preferred to multi-party synchronization, since in the cellular setting we typically have cells emitting a signal (active output action) and receptor cells (passive input action).

Consider the system in Figure 3, where two agents $\mathcal{A}$ and $\mathcal{B}$ are illustrated. Agent $\mathcal{A}$ can perform an output action $\overline{a}$ with rate λ; while $\mathcal{B}$ can perform the input actions (a, ω_1) and (a, ω_2). The relative selection probability of (a, ω_i) is calculated as the rate between ω_i and the total weight of a, that is the sum of the weights of all the enabled a-actions; in this example,

$$p(a, \omega_i) = \frac{\omega_i}{\omega_1 + \omega_2},\ i = 1, 2$$

Then, the *synchronization rate* between the actions (a, ω_i) and $(\overline{a}, \lambda)$ is given by $\lambda \cdot p(a, \omega_i)$.

Distance sensibility.

A fundamental property of agent-based models is the perception of the neighborhood. We embedded this feature in our simulator by allowing compatible agents to bind at distance. This method slightly differs from the theory of the Shape Calculus where binding between two 3D processes can exclusively occur when they share a common surface of contact.

More precisely, output bind actions are annotated with a parameter $d \in \mathbb{R}^+$ called *sensibility distance*, meaning that if an agent $\mathcal{A}$ can perform an action $(\overline{a}, \lambda)_d$, it can bind with any agent $\mathcal{B}$ which can perform a compatible action (a, ω) and which is distant from $\mathcal{A}$ at most d. In other words, it must hold that $d(\mathcal{A}, \mathcal{B}) = |\mathbf{p}(\mathcal{A}) - \mathbf{p}(\mathcal{B})| \leq d$, where $\mathbf{p}(\mathcal{A})$ ($\mathbf{p}(\mathcal{B})$) is the position of agent $\mathcal{A}$ ($\mathcal{B}$) in the 3D space. Figure 4 shows a context where an agent $\mathcal{A}$ is able to execute an

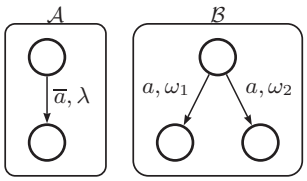

Figure 3: Agents synchronizing on compatible channels with stochastic rate λ and probability ω_i.

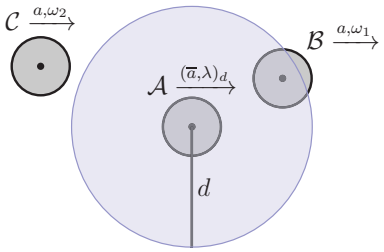

Figure 4: Agents exposing binding capabilities. Agent $\mathcal{C}$ is out of the perception radius of $\mathcal{A}$ (the blue circle), determined by the sensibility distance d. On the other hand, $\mathcal{A}$ can detect and bind with agent $\mathcal{B}$.

output bind action $(\overline{a}, \lambda)_d$. Even if $\mathcal{C}$ exposes a complementary channel, it is out of the perception radius of $\mathcal{A}$, which can consequently bind only with agent $\mathcal{B}$.
It is reasonable to expect that the actual distance between two agents affects their synchronization rate, since longer distances should lead to longer action durations. Therefore, we define the *binding rate* between two compatible bind actions $(\overline{a}, \lambda)_d$ and (a, ω) exposed by agents $\mathcal{A}$ and $\mathcal{B}$ respectively, by the ratio $\dfrac{\lambda \cdot p(a,\omega)}{d(\mathcal{A},\mathcal{B})}$.
The evolution of the system in our simulator is governed by a *race condition*: non-determinism is resolved by choosing among all the enabled actions the one with the highest rate. Depending on the type of action considered, i.e. an internal action, a synchronization (e.g. a split), or a binding, the mentioned rate would be a $\lambda \in \mathbb{R}^+$, the synchronization rate, or the binding rate, respectively.

The simulator for the BMU model is based on the *Repast Symphony Suite* [27], a Java-based environment for the specification and simulation of multi-agent systems. In particular, we have developed a library which allows the specification of Repast agents in a Shape Calculus-like syntax, as illustrated in Table 7. Thus, starting from the formal model, the user can define the different agents in the context in a straightforward way; the only concern is setting motion laws and extending the default classes, if necessary.
In the following we provide some details on the various components of the agent-based model and on its parameters (see Table 8). We will not focus on the stochastic rates and the weights of the actions, because we consider other sources of variability affecting the number of cells, their motion and

$$Oy \stackrel{\text{def}}{=} S_{Oy}[(\langle \mathsf{can}, \mathsf{X}\rangle + \langle \overline{\mathsf{can}}, \mathsf{X}\rangle)^{k_{Oy}} + \langle \mathsf{consume}, \mathsf{X}\rangle.\Theta]$$

```
NdPoint pos = new NdPoint(0,0,0);
NdPoint vel = new NdPoint(0,0,0);
Style3D points = new MySphere(radius);
Shape oy = new BasicShape(mass, pos, vel, points);
Channel c1 = new OutChannel("can", d_sens, rate);
Channel c2 = new InChannel("can", prob1);
Behaviour b1 = new Choice(new Bind(c1), new Bind(c2));
Behaviour b2 = new Iteration(b1, k_oy);
Channel c3 = new InChannel("consume", prob2);
Behaviour b3 = new Sequence(new Bind(c3), new Die());
oy.setBehaviour(new Choice(b2,b3));
```

Table 7: Translation of a 3D process in agent code.

Param	Value	Description
$size_{BMU}$	$2.4\times1.6\times0.01$ mm^3 [34]	Size of the BMU
Δ	1 day	Time step
k_{Oc}	2.5 days^{-1}	Resorption rate
k_{Ob}	0.25 days^{-1}	Formation rate
k_{RANKL}	$\in [1, 2]$	RANKL factor
k_{age}	$\in [1, 2]$	Aging factor

Table 8: Simulator parameters

their lifetime.

Spatial domain. We consider two different spatial domains, or *projections*: a continuous space and a discrete space, i.e. a grid. Space is approximated in two-dimensions, and has a size of $240 \times 160 \times 10^{-4}$ mm^2 (each cell in the grid models a portion of size 0.01×0.01 mm^2). According to the parameter $size_{BMU}$ in Table 8, we can ignore the depth of the BMU (0.01 mm) which is much smaller than its width (2.4 mm) and its height (1.6 mm). Including these projections has a two-fold utility: the continuous space allows to simulate fluid and realistic movements of the agents; on the other hand, the discretization of the space reduces the costs in computing the agent's neighborhood and its binding surfaces.

Time domain. As described in the theory of the Shape Calculus [3, 2], the time-line is divided in small segments of duration $\Delta \in \mathbb{R}^+$, called *movement time step*. After each Δ the velocities and the positions of all the shapes are updated, according to their particular motion law. For a matter of performances, those actions affecting the velocity and the positioning of shapes (e.g. bind and split actions) does not break the time-line before Δ has passed, differently from the Shape Calculus. Moreover in this setting, actions have an exponentially distributed duration. The scheduling policy for those actions is shown in Algorithm 1. In few words, if an action has a duration less than or equals to Δ, it is performed at Δ; otherwise, it is postponed to the subsequent time step. Given that a single remodeling cycle lasts about one year and the resorption and formation processes can take months, in this model Δ is set to 1 *day*.

Bone tissue. It is modeled as a real-valued matrix *Bone*. The value of a cell $Bone_{ij}$ represents the percentage bone density at the position (i, j) of the BMU grid, and varies from 0 (void) to 1 (fully mineralized).

Algorithm 1 Algorithm for scheduling stochastic actions and updating the time-line.

$t \leftarrow 0$
Let $L = \{l_0, \ldots, l_n\}$ be a list of (a, X)-couples $(action, duration)$, in ascending order w.r.t. durations
while $t \leq t_{max}$ **do**
  Calculate all the (a, X)-couples to execute and add them to L, s.t. (a, X) does not involve an agent already having an action in L
  while $L \neq \emptyset \wedge ((a, X) \leftarrow l_0) \leq \Delta$ **do**
    execute a
    $L \leftarrow L \setminus \{l_0\}$
  end while
  $i \leftarrow 0$
  while $l_i \in L$ **do**
    $(a, X) \leftarrow l_i$
    $L \leftarrow L \setminus \{l_i\} \cup \{(a, X - \Delta)\}$
    $i \leftarrow i + 1$
  end while
  update velocities and positions
  $t \leftarrow t + \Delta$
end while

Osteocytes. We assume that osteocytes are located nearby the micro-fracture, and produce RANKL in order to attract osteoclasts to the portion of bone to repair.

Osteoclasts. In normal conditions, the number of osteoclasts in the BMU is subject to little variation from the average $n_{Oc} = 20$. Higher perceived densities of RANKL in the environment, which are caused by an inflammation or a signaling defect, lead to a higher production of osteoclasts. Their motion law is the combination of a random walk and of the RANKL attraction. The expected lifetime t_{Oc} is 10 days, but they can undergo apoptosis before t_{Oc} if a high concentration of osteoblasts is detected in the neighborhood. Once reached the portion of bone to consume, an osteoclast reduces the percentage density in that part of bone of $k_{Oc} = 2.5$ each day.

Osteoblasts. The number of osteoblasts in the system varies randomly with an average $n_{Ob} = 2000$. Similarly to osteoclasts, the motion of osteoblasts is regulated by random movements and by attraction factors; in particular, they are directed towards the nearest point to mineralize. Moreover, osteoblast precursors emit RANKL which contributes to osteoclasts' production and stimulation. Mature osteoblasts inhibits this RANKL signaling with the production of OPG. The lifetime of an osteoblast is about 20 days: 5 days as a precursor, 15 days as a mature cell active in the formation process. When active, it increases the bone density of a factor $k_{Ob} = 0.25$ each day. It can die before its lifetime has passed, if the number of active osteoclasts in the system is higher than expected. Finally, we assume that osteoblasts are recruited only after that the concentration of osteocytes' RANKL goes below a fixed threshold.

RANKL. At the simulation level, RANKL is not merely a channel exposed by osteocytes or osteoblasts. In fact, those signals produce in a combined way a scalar field modeling the concentration of RANKL in the BMU. It is such that osteoclasts' movement is determined by the *gradient* of that scalar field. Hence at the specification level, signals are modeled as communication channels. At the implementation level, output channels are assumed to produce signals which diffuse in the space and attract agents exposing compatible input channels.

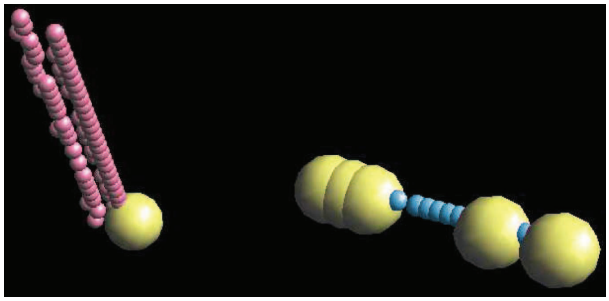

Figure 5: Screenshot of the BMU during a simulation. We assume that the connection with blood and marrow - i.e. where cells are generated - is located in the left part of the BMU. Osteocytes (blue spheres) are located along the microfracture. Osteoclasts (yellow) are attracted by and bind with osteocytes. At this stage, osteoblasts (red spheres on the left) are being recruited to start the formation phase. Other structures such the hydroxyl apatite backbone are not represented.

A prototype of the simulator is available in the form of a Repast project at `http://cosy.cs.unicam.it/ubiolab/BR.zip`.

5. RESULTS

The aim of this work is to show how apparently insignificant changes in RANKL signaling lead to disease conditions, especially when aging factors are involved. In particular, we defined two configurations by varying the parameters k_{RANKL} and k_{age} (see Table 8):

- **healthy conf.** ($k_{RANKL} = 1$, $k_{age} = 1$), where RANKL production and cellular activity is normal;
- **osteoporotic conf.** ($k_{RANKL} = 2$, $k_{age} = 2$), with an overproduction of RANKL and a reduced cellular activity.

When running the osteoporotic configuration, higher values of RANKL induce a higher production of osteoclasts, hence to a higher resorption activity. The aging factor is responsible for a reduced osteoblastic activity which is not sufficient to completely repair the consumed part of bone. This causes a lower total bone density, weaker trabeculae and consequently more frequent and more consistent microfractures in osteoporotic patients.
It is worth noticing that when the aging factor is absent (e.g. in a young patient), an overproduction of RANKL don't determine a disease situation; an unexpected high resorption activity can be easily balanced by increasing the number of osteoblasts and their formation rate, which is not possible in

an old patient. Conversely, with a regular RANKL signaling, weaker osteoclasts are balanced by weaker osteoblasts; hence, even older patients are not subject to relevant negative remodeling phenomena.
Figure 6 illustrates the snapshots taken during the simulation of the two configurations, at time:

$t = 130$: osteoclasts (yellow spheres) are nearby osteocytes (blue) along the micro-fracture, and consume bone surface, forming the black cavities visible in the second row. The first osteoblasts (red spheres) are recruited and start mineralizing cavities on the left part of the micro-fracture. In this phase, RANKL production is at its maximum, because of the combined signaling of osteocytes and pre-osteoblasts in the BMU. Note that while the bone density is approximately the same between the healthy and the osteoporotic configurations, the RANKL concentration is much higher in the second case.

$t = 350$: the remodeling cycle is in its final days. Differences in the bone density are quite prominent: in Figure 6 (f) the damage has almost been repaired; while Figure 6 (h) shows how the reduced osteoblastic activity generates several zones with a lower bone density. In addition, since the number of osteocytes and pre-osteoblasts in the BMU decreases, we notice a minor RANKL production.

Figure 7 shows the average cumulative values of bone resorption and formation for the healthy configuration (Fig. 7 (a)), and for the osteoporotic configuration (Fig. 7 (b)). In Fig. 8 (a) and (b), we compared the values of the percentage bone density obtained by running the two configurations.

6. DISCUSSION AND CONCLUSION

In this paper, we provided a modeling framework consisting of a process-algebraic specification layer and a agent-based implementation layer for describing the process of bone remodeling. The formal specification in the language of the Shape Calculus follows the almost unexplored paradigm of *processes as cells* and takes into account also spatial and physical aspects, which prominently affect the dynamics of bone remodeling and more generally, of any biological system, from the molecular scale to the tissue scale.
A large variety of computational formalisms equipped with spatial capabilities have been proposed so far (see [4] for an exhaustive review), such as rewrite systems [31, 15, 1, 11], and cellular automata [9]. In the field of process algebras, compartmentalization is a common way to represent process localization [10, 33, 30, 7]; recent works address the problem of expressing also more complex spatial features [8, 19, 35, 3], by enriching the classical notion of process with physical information, position and movement in discrete or continuous coordinate systems, geometry and geometrical transformations.
Besides the good expressiveness of spatial properties, the novelty of the proposed methodology with respect to the above-cited formalisms is the connection between the high-level formulation in the Shape Calculus with the low-level stochastic agent-based simulation in Repast: 3D networks are "implemented" as multi-agent systems in a natural and extensible way.
Furthermore, the formal modeling of bone remodeling is a challenging field of research, since the actual knowledge of

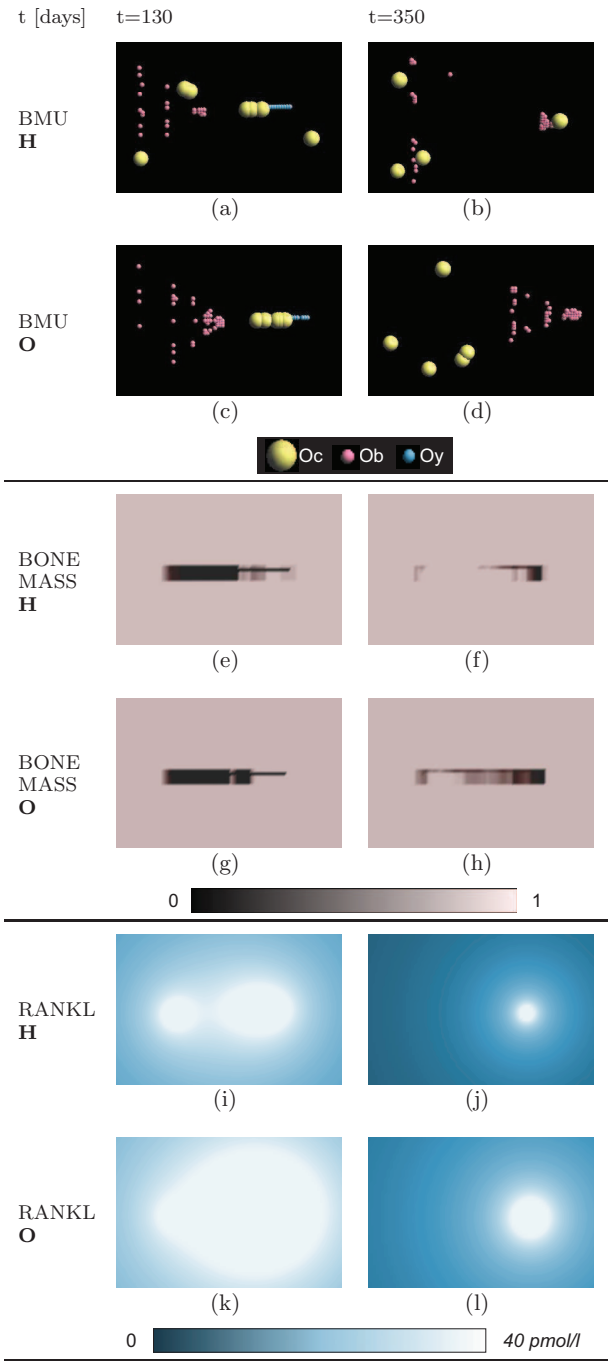

Figure 6: Simulation of healthy (H) and osteoporotic (O) configurations. The first row displays the position of the agents (the cells) in the context (the BMU); pictures in the second row represent the bone density; the third row illustrates the RANKL concentration in the environment. The spatial domain is determined by the extent of the BMU ($2.4 \times 1.6\ mm^2$).

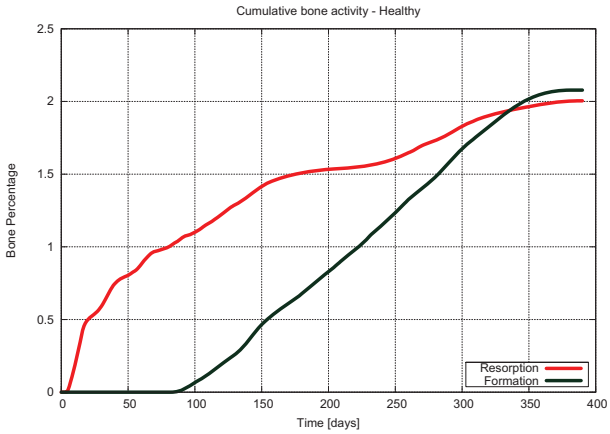

(a) Healthy configuration

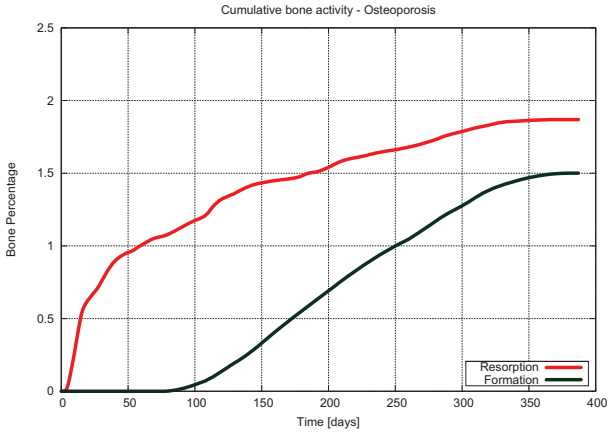

(b) Osteoporotic configuration

Figure 7: Cumulative bone activity. The top graph shows that in healthy conditions the formation phase (green line) compensate the resorption one (red line). On the other hand, in the disease scenario formation is not effective enough, even if the resorption activity is not greater than in the healthy case. This is attributable to the combination of aging factors leading to reduced resorption and formation rates, and an overproduction of RANKL which attracts a higher number of osteoclasts in the BMU.

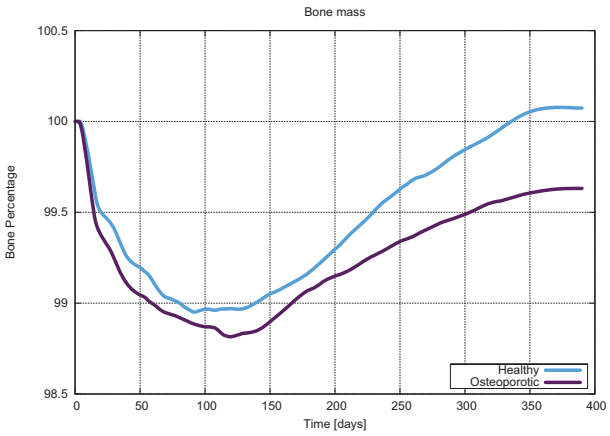

(a) Average bone density

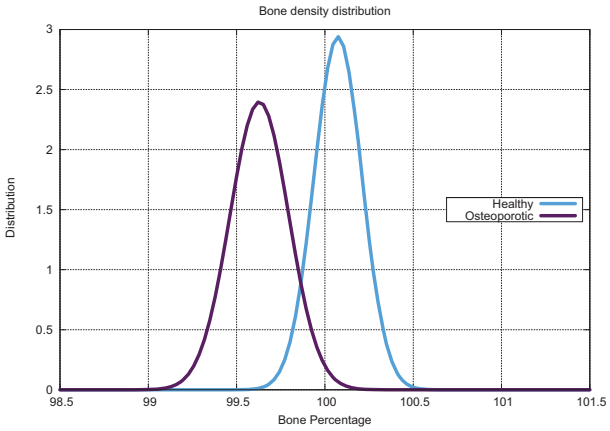

(b) Bone density distribution

Figure 8: Comparison of the results of healthy and osteoporotic configurations. Top graph displays the bone density values during a single remodeling cycle. In normal conditions, at the end of remodeling the initial bone density is reestablished. In the case of osteoporosis, the minimal values of percentage density are reached during resorption, and the final density is lower than the initial one. The bottom graph compares the normal distributions obtained from the results of twenty simulations.

this process at cellular level has still several obscure points. Whereas the most important current efforts in bone remodeling are based on continuous mathematics (recently reviewed in [28]), primarily ODE and PDE, our individual-based model rely on a theoretically formal framework and results more biologically sound, since it combines the discrete and stochastic evolution of cells with a three-dimensional continuous spatial domain. We report that our simulation is time-consistent with the real biological process and that the results obtained agree with previous well-established literature, in particular with [21] (ODE model) and with [34] (PDE model). In addition, we succeeded in reproducing the homeostatic nature of bone remodeling by running a "healthy" configuration, as well as simulating bone diseases like osteoporosis, by running a "sick" configuration characterized by a RANKL signaling defect and by aging factors. There are other recent attempts worth being mentioned [22, 6, 5] in which computational formalisms are employed to describe bone remodeling.

Despite the convincing results achieved, this is only the starting point of our research project, and we are planning to extend our work in several future directions.

We intend to enrich the biological model by incorporating details of the intracellular pathway network, and of biomechanical aspects in bone tissue. Then, a great challenge would be using our simulator to test the effects of experimental drugs, or to simulate how the organism responds to the implant of artificial bone tissue.

Another avenue for future research is verifying properties related to bone density and bone pathologies through a model checking approach. Assuming that we know the conditions of the system that could be identified through medical investigations, we aim to answer questions such as "How long, from the a current state, will the system take to repair a fracture?", or "Which is the probability that the system will reach a state where the bone density is below a critical threshold?"

Acknowledgment

Pietro Liò thanks RECOGNITION: *Relevance and cognition for self-awareness in a content-centric Internet (257756)*, which is funded by the European Commission within the 7^{th} Framework Programme (FP7).

7. REFERENCES

[1] R. Barbuti, A. Maggiolo-Schettini, P. Milazzo, G. Pardini, and L. Tesei. Spatial p systems. *Natural Computing*, pages 1–14, 2010.

[2] E. Bartocci, D. Cacciagrano, M. Di Berardini, E. Merelli, and L. Tesei. Timed Operational Semantics and Well-Formedness of Shape Calculus. *Scientific Annals of Computer Science*, 20, 2010.

[3] E. Bartocci, F. Corradini, M. Di Berardini, E. Merelli, and L. Tesei. Shape Calculus. A Spatial Mobile Calculus for 3D Shapes. *Scientific Annals of Computer Science*, 20, 2010.

[4] A. T. Bittig and A. M. Uhrmacher. Spatial modeling in cell biology at multiple levels. In J. M.-T. J. H. B. Johansson, S. Jain and E. YÃijcesan, editors, *Proceedings of the 2010 Winter Simulation Conference*, pages 608–619. IEEE, 2010.

[5] D. Cacciagrano, F. Corradini, and E. Merelli. Bone remodelling: A complex automata-based model running in bioshape. In S. Bandini, S. Manzoni, H. Umeo, and G. Vizzari, editors, *Cellular Automata*, volume 6350 of *Lecture Notes in Computer Science*, pages 116–127. Springer Berlin / Heidelberg, 2010.

[6] D. Cacciagrano, F. Corradini, E. Merelli, and L. Tesei. Multiscale bone remodelling with spatial p systems. In *Proceedings Compendium of the Fourth Workshop on Membrane Computing and Biologically Inspired Process Calculi*. book-on-demand. de, 2010.

[7] L. Cardelli. Brane calculi. In *Computational methods in systems biology*, pages 257–278. Springer, 2005.

[8] L. Cardelli and P. Gardner. Processes in space. In *Programs, Proofs, Processes*, volume 6158 of *Lecture Notes in Computer Science*, pages 78–87. Springer Berlin / Heidelberg, 2010.

[9] B. Chopard and M. Droz. *Cellular automata modeling of physical systems*. Cambridge University Press Cambridge, UK, 1998.

[10] F. Ciocchetta and M. L. Guerriero. Modelling biological compartments in bio-pepa. *Electron. Notes Theor. Comput. Sci.*, 227:77–95, January 2009.

[11] V. Danos, J. Feret, W. Fontana, R. Harmer, and J. Krivine. Rule-based modelling of cellular signalling. *CONCUR 2007–Concurrency Theory*, pages 17–41, 2007.

[12] R. De Nicola, D. Latella, M. Loreti, and M. Massink. Rate-based transition systems for stochastic process calculi. *Automata, Languages and Programming*, pages 435–446, 2009.

[13] D. Epari, G. Duda, and M. Thompson. Mechanobiology of bone healing and regeneration: in vivo models. *Proceedings of the Institution of Mechanical Engineers, Part H: Journal of Engineering in Medicine*, 224(12):1543–1553, 2010.

[14] X. Feng and J. McDonald. Disorders of Bone Remodeling. *Annual review of pathology*, 2010.

[15] J. Giavitto. Topological collections, transformations and their application to the modeling and the simulation of dynamical systems. In *Rewriting Techniques and Applications*, pages 208–233. Springer, 2003.

[16] R. Hanada, T. Hanada, and J. Penninger. Physiology and pathophysiology of the RANKL/RANK system. *Biological Chemistry*, 391(12):1365–1370, 2010.

[17] J. Hillston. *A compositional approach to performance modelling*. Number 12. Cambridge Univ Pr, 1996.

[18] S. Jabbar, J. Drury, J. Fordham, H. Datta, R. Francis, and S. Tuck. Osteoprotegerin, RANKL and bone turnover in postmenopausal osteoporosis. *Journal of Clinical Pathology*, 64(4):354, 2011.

[19] M. John, C. Lhoussaine, J. Niehren, and A. Uhrmacher. The attributed π-calculus with priorities. *Transactions on Computational Systems Biology XII*, pages 13–76, 2010.

[20] G. Karsenty and F. Oury. The central regulation of bone mass, the first link between bone remodeling and energy metabolism. *Journal of Clinical Endocrinology & Metabolism*, 95(11):4795, 2010.

[21] S. Komarova, R. Smith, S. Dixon, S. Sims, and L. Wahl. Mathematical model predicts a critical role for osteoclast autocrine regulation in the control of

bone remodeling. *Bone*, 33(2):206–215, 2003.

[22] L. Li and H. Yokota. Application of petri nets in bone remodeling. *Gene Regulation and Systems Biology*, 3:105, 2009.

[23] P. Lió, E. Merelli, N. Paoletti, and M. Viceconti. A combined process algebraic and stochastic approach to bone remodeling. In *CS2BIO 2011. Accepted*, 2011.

[24] S. Manolagas and A. Parfitt. What old means to bone. *Trends in Endocrinology & Metabolism*, 21(6):369–374, 2010.

[25] R. Milner. *A calculus of communicating systems*, volume 92. Springer-Verlag, 1980.

[26] N. Morabito, A. Gaudio, A. Lasco, M. Atteritano, M. A. Pizzoleo, M. Cincotta, M. La Rosa, R. Guarino, A. Meo, and N. Frisina. Osteoprotegerin and rankl in the pathogenesis of thalassemia-induced osteoporosis: New pieces of the puzzle. *Journal of Bone and Mineral Research*, 19(5):722–727, 2004.

[27] M. North, T. Howe, N. Collier, and J. Vos. A Declarative Model Assembly Infrastructure for Verification and Validation. In *Advancing Social Simulation: The First World Congress*, pages 129–140. Springer Japan, 2007.

[28] P. Pivonka and S. Komarova. Mathematical modeling in bone biology: From intracellular signaling to tissue mechanics. *Bone*, 47(2):181–189, 2010.

[29] G. Plotkin. *A structural approach to operational semantics*. 1981.

[30] C. Priami and P. Quaglia. Beta binders for biological interactions. In V. Danos and V. Schachter, editors, *Computational Methods in Systems Biology*, volume 3082 of *Lecture Notes in Computer Science*, pages 20–33. Springer Berlin / Heidelberg, 2005.

[31] G. Pun. Computing with membranes. *Journal of Computer and System Sciences*, 61(1):108–143, 2000.

[32] L. Raggatt and N. Partridge. Cellular and molecular mechanisms of bone remodeling. *Journal of Biological Chemistry*, 285(33):25103, 2010.

[33] A. Regev, E. M. Panina, W. Silverman, L. Cardelli, and E. Shapiro. Bioambients: an abstraction for biological compartments. *Theoretical Computer Science*, 325(1):141 – 167, 2004. Computational Systems Biology.

[34] M. Ryser, N. Nigam, and S. Komarova. Mathematical Modeling of Spatio-Temporal Dynamics of a Single Bone Multicellular Unit. *Journal of bone and mineral research*, 24(5):860–870, 2009.

[35] A. Stefanek, M. Vigliotti, and J. T. Bradley. Spatial extension of stochastic π calculus. In *8th Workshop on Process Algebra and Stochastically Timed Activities*, pages 109–117, August 2009.